KIF16B mediates anterograde transport and modulates lysosomal degradation of the HIV-1 envelope glycoprotein

Nicholas Weaver,[a,b] Jason Hammonds,[b] Lingmei Ding,[b] Grigoriy Lerner,[a,b] Krista Dienger-Stambaugh,[b] Paul Spearman[b]

[a]Immunobiology Division, Cincinnati Children's Hospital Medical Center and the University of Cincinnati

[b]Infectious Diseases, Cincinnati Children's Hospital Medical Center and the University of Cincinnati

ABSTRACT

The human immunodeficiency virus type 1 (HIV-1) envelope glycoprotein (Env) is incorporated into virions at the site of particle assembly on the plasma membrane (PM). The route taken by Env to reach the site of assembly and particle incorporation remains incompletely understood. Following initial delivery to the PM through the secretory pathway, Env is rapidly endocytosed, suggesting that recycling is required for particle incorporation. Endosomes marked by the small GTPase Rab14 have been previously shown to play a role in Env trafficking. Here we examined the role of KIF16B, the molecular motor protein that directs outward movement of Rab14-dependent cargo, in Env trafficking. Env colocalized extensively with KIF16B+ endosomes at the cellular periphery, while expression of a motor-deficient mutant of KIF16B redistributed Env to a perinuclear location. The half-life of Env labeled at the cell surface was markedly reduced in the absence of KIF16B, while a normal half-life was restored through inhibition of lysosomal degradation. In the absence of KIF16B, Env expression on the surface of cells was reduced, leading to a reduction in Env incorporation into particles and a corresponding reduction in particle infectivity. HIV-1 replication in KIF16B knockout cells was substantially reduced as compared to wildtype cells. These results indicate that KIF16B regulates an outward sorting step involved in Env trafficking, thereby limiting lysosomal degradation and enhancing particle incorporation.

IMPORTANCE The HIV-1 envelope glycoprotein is an essential component of HIV-1 particles. The cellular pathways that contribute to incorporation of envelope into particles are not fully understood. Here we identify KIF16B, a motor protein that directs movement

38 from internal compartments toward the plasma membrane, as a host factor that prevents
39 envelope degradation and enhances particle incorporation. This is the first host motor
40 protein identified that contributes to HIV-1 envelope incorporation and replication.

41

42 **INTRODUCTION**

43 The HIV-1 Env protein plays critical roles in the viral lifecycle, mediating receptor and
44 coreceptor binding, fusion, and entry into target cells. Env is the principal neutralizing
45 determinant on the surface of virions, and has been a primary focus of vaccine design
46 efforts since the onset of the HIV pandemic. While many aspects of Env structure and
47 function are now understood, the determinants of particle incorporation of Env are not
48 fully defined. HIV-1 Env is synthesized on endoplasmic reticulum (ER)-bound ribosomes
49 as a precursor gp160 protein. Trimerization and initial glycosylation of Env take place in
50 the ER, followed by additional glycan modifications and cleavage of gp160 into gp120
51 (SU) and gp41 (TM) subunits in the Golgi apparatus. After delivery to the PM, the
52 heterotrimeric Env complex is rapidly endocytosed into early endosomes (1-3). The
53 trafficking events that occur following Env endocytosis are poorly defined, and are the
54 subject of this report.

55 Clues to Env trafficking and particle incorporation have come from studies of the Env
56 cytoplasmic tail (CT). Long CTs are a characteristic feature of most lentiviral Env proteins.
57 HIV-1, HIV-2, and simian immunodeficiency virus (SIV) have Env CTs of approximately
58 150 amino acids. The CT of HIV-1 Env contains multiple functional motifs that have been
59 implicated in intracellular trafficking events [reviewed in (4, 5)], suggesting that the CT
60 interacts with host trafficking molecules to direct intracellular trafficking and particle
61 incorporation of Env. In support of the critical role of the CT, Murakami and Freed showed
62 that there are remarkable cell type-specific differences in incorporation of Env with a large
63 deletion in the CT (6). While some cell lines such as MT-4 and 293T cells readily
64 incorporate Env bearing a truncated CT, incorporation into virions in most T cell lines, in

65 primary T lymphocytes, and in monocyte-derived macrophages (MDMs) requires an intact
66 CT (6-9). HeLa cells demonstrate an intermediate phenotype, with a reduction but not
67 complete loss of Env incorporation with a CT truncation (6). The cell type-dependent
68 incorporation of Env with a truncated CT, together with evidence supporting trafficking
69 motifs within the CT, suggests that specific host factors are required for incorporation of
70 Env into particles.

71 We previously demonstrated that a Rab-related adaptor protein Rab11-FIP1C
72 (FIP1C) plays a role in Env incorporation, and outlined a key role for recycling pathways
73 in this process (10-12). The specific Rab GTPase involved in FIP1C-mediated recycling
74 of Env was shown to be Rab14 (10). Additional evidence supporting a role for Rab14
75 comes from Hoffman and colleagues, who demonstrated that Env traffics to Rab14+ late
76 endosomes and lysosomes (13). Recycling of Env to the PM was demonstrated in this
77 study, and a potential role for Rab14 in regulating lysosomal degradation vs. delivery to
78 the PM was suggested. Given the accumulating evidence for Rab14 in the intracellular
79 trafficking of Env, we sought to evaluate the role of the molecular motor protein that
80 associates with Rab14, KIF16B.

81 KIF16B is a member of the kinesin-3 family of molecular motor proteins. KIF16B is a
82 plus end-directed molecular motor that regulates the steady-state distribution of Rab5+
83 early endosomes and plays a role in recycling of endocytosed cargo to the cell surface
84 (14). A seminal study describing KIF16B function demonstrated that disruption of KIF16B
85 led to redistribution of epidermal growth factor receptor (EGFR) and enhanced its
86 degradation in the lysosome (14). KIF16B has also been implicated in anterograde
87 transport of transferrin receptor and fibroblast growth factor receptor (FGFR), in

88 contributing to MHC class I cross-presentation, and in directing apical transcytosis of
89 cargo in epithelial cells (14-17). KIF16B binds directly to Rab14, and a Rab14-KIF16B
90 complex has been shown to be essential for transport of FGFR and in mediating antigen
91 cross-presentation by dendritic cells (15, 16). Given the role of Rab14 in HIV-1 Env
92 trafficking, we hypothesized that KIF16B-mediated transport plays a role in anterograde
93 trafficking of Env. We found that KIF16B directs Env to early endosomes located at the
94 periphery of cells, while expression of a motor-deficient KIF16B molecule retained Env in
95 perinuclear endosomal compartments. Measurement of the half-life of Env in KIF16B
96 knockout (KO) cells revealed an enhanced rate of Env degradation that could be reversed
97 using an inhibitor of lysosomal acidification. Knockout of KIF16B expression in a T cell
98 line diminished cell surface levels of Env incorporation, Env incorporation into particles,
99 particle infectivity, and viral replication in a spreading infection. These studies implicate
100 KIF16B in anterograde movement of Env away from degradation in the lysosome,
101 allowing more efficient incorporation into HIV-1 particles.

102

103 **RESULTS**

104 **Env localizes to KIF16B-positive compartments and is redistributed by**
105 **dominant-negative KIF16B overexpression.** To determine if HIV-1 Env is found in
106 KIF16B-positive endosomal compartments, we co-expressed the HIV-1 NL4-3 Env with
107 KIF16B tagged with yellow fluorescent protein (YFP) in HeLa cells. KIF16B+
108 compartments were readily observed at the periphery of cells and demonstrated a striking
109 colocalization with Env (Fig. 1A). Expression of KIF16B bearing a mutation in the
110 nucleotide binding motif that disrupts its motor function, KIF16B-S109A-YFP, has been

111 shown to act in a dominant-negative fashion to impair EGFR trafficking (14). Similar to
112 what was seen with EGFR, HIV-1 Env was redistributed by expression of KIF16B-S109A-
113 YFP to a perinuclear location (Fig. 1B). Expression of Env from intact NL4-3 proviral DNA
114 together with wildtype KIF16B led to a peripheral distribution of Env, similar to that seen
115 upon expression of Env alone (Fig. 1C). Expression of intact provirus with KIF16B-S109A-
116 YFP also revealed relocalization of Env to a perinuclear location (Fig. 1D). To quantify
117 the observed difference in subcellular localization, we used a mask 30% the distance from
118 the outer edge at the periphery of the cell to the stained nucleus, and measured Env
119 signal within this mask as compared to total Env signal in the cell. 40 cells were examined
120 for this analysis. The significant differences in peripheral localization shown in the
121 representative images were confirmed quantitatively, as shown in Fig. 1E. Expression of
122 either WT or S109A KIF16B resulted in a high degree of colocalization with Env, as
123 measured by Pearson's coefficient (Fig. 1F). We noted a somewhat higher degree of
124 colocalization with KIF16B-S109A-YFP expression, which was statistically significant
125 when Env alone was expressed (Fig. 1F). These results largely mirror results reported for
126 KIF16B relocalization of EGFR (14), and support the hypothesis that KIF16B promotes
127 anterograde transport of Env in early endosomal compartments.

128 **KIF16B fails to redistribute heterologous viral glycoproteins.** We considered the
129 possibility that overexpression of KIF16B could divert early endosomes to the periphery
130 of cells in a non-specific manner that would be seen with other viral envelope
131 glycoproteins. To address this possibility, we examined the effect of expression of WT vs.
132 S109A KIF16B on the distribution of three unrelated viral glycoproteins: influenza
133 glycoprotein hemagglutinin (HA), Ebola virus glycoprotein (EBOV GP), and severe acute

134 respiratory syndrome coronavirus 2 spike (SARS-CoV-2 S) protein. As noted previously,
135 WT KIF16B was consistently found at the periphery of cells, while KIF16B-S109A
136 localized near the cell nucleus. No redistribution of HA, EBOV GP, or SARS-CoV-2 S was
137 seen for KIF16B vs. KIF16B-S109A expression (Fig. 2A-F). Furthermore, in contrast to
138 HIV-1 Env, these heterologous viral glycoproteins failed to colocalize significantly with
139 KIF16B as indicated by visual inspection and by determination of a slightly negative
140 Pearson's Coefficient (supplemental Fig. S1C). These results demonstrate that HIV-1 Env
141 colocalization with and redistribution by KIF16B is not widely generalizable to viral
142 glycoproteins, at least as indicated by examination of a paramyxovirus, filovirus, and
143 coronavirus envelope glycoprotein. Next, we examined the effects of expression of
144 KIF1B, a closely related kinesin mediating plus end-directed trafficking, or its dominant
145 negative (motor-deficient) form KIF1B-Q98L (18), on HIV-1 Env distribution. KIF1B was
146 found at the cellular periphery, while and KIF1B-Q98L localized to perinuclear locations
147 in a manner similar to that of KIF16B and KIF16B-S109A (supplemental Fig. S1A, 1B).
148 However, distribution of HIV-1 Env did not appear to shift to the periphery or perinuclear
149 region upon expression of KIF1B and KIF1B-Q98L, respectively (Fig. S1A, 1B). In
150 contrast to results with KIF16B, Env was not significantly colocalized with either KIF1B
151 protein (Fig. S1C). Together, these results suggest that KIF16B plays a specific role in
152 anterograde trafficking of HIV-1 Env.

153 **HIV-1 Env on the PM is endocytosed into KIF16B positive endosomes.** The
154 studies described above examined the total pool of Env in the cell, and did not study the
155 endocytosed pool of Env in isolation. In order to determine if Env is delivered into KIF16B
156 positive endosomes directly from the PM, we utilized a novel approach using flourogen

157 activating protein (FAP) tagging (19). The FAP tag was placed within the V2 loop of the
158 ectodomain of JR-FL Env as illustrated in Fig. 3A, creating the FAP-Env construct. To
159 validate this system for use in assessing Env incorporation, we examined particle
160 incorporation of FAP-Env. FAP-Env was co-expressed with Env-deficient provirus, and
161 was efficiently incorporated into virions as indicated by Western blot analysis
162 (supplemental Fig. S2). Combining expression of this construct (FAP-Env) with a
163 flourogen impermeant to the PM (MG-11p, αRED-np1 from Spectragenetics) allowed
164 visualization of the fate of pulse-labeled Env present on the surface of cells. We first co-
165 expressed FAP-Env with KIF16B WT in HeLa cells and fixed the cells after pulse labeling
166 them on ice to visualize the surface staining in the absence of endocytosis. Fig. 3B
167 demonstrates that the cell membrane-impermeable reagent fluoresced upon binding to
168 Env on the cell surface and did not penetrate the PM. We next allowed internalization of
169 FAP-Env for 15 minutes at 37°C after pulse-labeling, and found that surface-labelled FAP-
170 Env on the surface had accumulated into KIF16B-positive compartments (Fig. 3B). We
171 also performed the same experiment with KIF16B S109A and found similar results (Fig.
172 3C). In order to follow the movement of this FAP-Env population expressed on the cell
173 surface in real-time, we pulse-labeled FAP-Env and recorded live-cell video of Env
174 movement into HeLa cells expressing KIF16B or KIF16B-S109A. Pulse-labeled Env was
175 endocytosed within a few minutes and demonstrated increasing colocalization with
176 KIF16B+ endosomes at the periphery of cells, or with KIF16B-S109A+ endosomes in the
177 perinuclear region of the cell (Fig. 3D and 3E, and supplemental video 1 and 2). These
178 results demonstrate that HIV-1 Env on the surface of the cell is rapidly endocytosed and
179 thereafter accumulates in KIF16B+ endosomes.

180 **Deletion of KIF16B leads to enhanced degradation of Env and accumulation**
181 **within the lysosome.** It has been established that KIF16B-mediated transport can divert
182 cellular cargo from default pathways that lead to lysosomal degradation, while depletion
183 of KIF16B enhances their degradation (14, 16) We therefore hypothesized that a loss of
184 normal anterograde trafficking of Env mediated by KIF16B could result in enhanced Env
185 degradation. To evaluate this possibility, we utilized CRISPR/Cas9 technology to
186 knockout KIF16B in both HeLa cells and H9 T cells, followed by characterization of
187 isolated cell clones. Fig. S3 shows characterization of one HeLa and one H9 clone used
188 for subsequent studies, and is consistent with the findings from several clones examined
189 for each cell type. Note the complete absence of KIF16B by Western blotting in
190 supplemental Fig. S3A. We then utilized the KIF16B KO HeLa cell clones together with
191 pulse-labeling of Env using the FAP tag technique described above. FAP-Env was
192 expressed in WT or KIF16B KO cells, and the kinetics of disappearance of total cellular
193 FAP-Env signal was measured over time. These experiments were controlled for the
194 effects of photobleaching on FAP-Env signal as outlined in Materials and Methods.
195 Remarkably, the FAP-Env signal degraded at a considerably faster rate in KIF16B KO
196 cells than in WT cells (images in Fig. 4A vs. Fig. 4B and supplemental video 3). The half-
197 life of endocytosed Env measured in WT HeLa cells by this method was 159.5 minutes
198 (95% C.I. 145.4 – 175.6), while in the absence of KIF16B Env was more rapidly degraded,
199 with a half-life of 56.9 minutes (95% C.I. 54.1 – 59.8). Furthermore, when we incubated
200 KIF16B KO cells with lysosomal inhibitor bafilomyacin-A1 (Baf-A1), the degradation rate
201 in KIF16B KO cells returned to wild-type levels (Fig. 4 A, B, C, E and supplemental video
202 3). To corroborate the observation that KIF16B knockout leads to enhanced degradation

203 of Env as measured by degradation of FAP-tagged Env, we performed surface pulse-
204 labeling with NHS-biotin in WT and KIF16B KO HeLa cells on ice, followed by quenching
205 of remaining biotin and pulldown of internalized biotinylated proteins with streptavidin
206 beads at multiple timepoints following incubation at 37°C. Detection of internalized Env
207 was then performed using quantitative Western blotting. Figure 4D shows Western blot
208 examples representative of results from five individual experiments for each experimental
209 arm. As compared with WT cells, pulse-labeled Env in KIF16B KO cells was more rapidly
210 degraded (Fig. 4D, compare WT to KO blots). The addition of Baf-A1 reduced the
211 degradation to essentially WT levels (Fig. 4D, 4F). Using repeated experiments, we
212 generated degradation curves for pulsed Env in WT, KO, and KO + Baf-A1 cells that were
213 similar, but not identical, to the curves derived from FAP-Env labeling (Fig. 4F, compare
214 to 4E). Env half-life measured by this method was 154.1 minutes for WT cells, 32.1
215 minutes for KO cells, and 94.9 minutes for Baf-A1-treated KO cells. While we noted that
216 the results were not identical between the two methods employed, they are in good
217 general agreement, and establish that KIF16B KO leads to more rapid Env degradation
218 that can be rescued by Baf-A1. Together, these results clearly show that KIF16B limits
219 lysosomal degradation of Env, likely through promoting anterograde trafficking.

220 Given results above with the lysosomal inhibitor Baf-A1, we sought to determine if the
221 absence of KIF16B results in a shift in Env distribution into the lysosomal compartment.
222 Results of immunofluorescence staining were striking. WT HeLa cells revealed punctate
223 lysosomes with a moderate degree of Env colocalization, while intracellular Env was
224 clearly distinguished outside of the lysosome (marked by LAMP1 staining) (Fig. 5A). In
225 KIF16B KO cells, Env colocalization with LAMP1 was dramatically higher (Fig. 5B and

226 5D). Baf-A1 treatment of KIF16B KO cells did not show significant differences in
227 colocalization of Env and LAMP1 as compared with untreated KO cells, as both showed
228 very high levels of colocalization as quantified by Pearson's coefficient (Fig. 5C and 5D).
229 Taken together, these results from imaging and pulse-chase analysis suggest that
230 deletion of KIF16B increases the rate of Env degradation due to loss of anterograde
231 movement normally conferred by KIF16B, resulting in shunting to the lysosome for
232 degradation.

233 **KIF16B deletion leads to defects in Env incorporation, particle infectivity, and**
234 **viral replication.** We next examined the effect of KIF16B depletion on Env trafficking and
235 incorporation into particles. We first assessed surface levels of Env by flow cytometry
236 after infecting WT or KIF16B KO H9 cells with NL4-3 virus. Surface expression levels of
237 Env were consistently diminished in KIF16B KO cells compared with WT cells (Fig. 6A
238 and 6B), consistent with diminished anterograde movement of Env. Total cellular Env
239 measured by flow cytometry was also diminished, but to a somewhat lesser degree than
240 cell surface Env (Fig. 6B). This result is consistent with the enhanced lysosomal
241 degradation of endocytosed Env shown in prior results. Viruses were then purified from
242 supernatants of infected WT and KIF16B KO H9 cells, in order to examine levels of Env
243 incorporation into particles. Viral particle Env content was significantly reduced in KIF16B
244 KO cells compared to WT H9 (>50% reduction from wild-type levels as quantified by LI-
245 COR Image Studio Software, n = 5) (Fig. 6C). The leftmost blot in Fig. 6C shows particle
246 Env content normalized by equal p24 content loading of the lanes. When cell lysates were
247 examined following multiple rounds of replication in WT or KIF16B KO cells and
248 normalized for total protein, there was a reduction of all viral proteins, reflecting

249 diminished replication (Fig. 6C, cell lysate). Notably, however, production of gp160 in
250 KIF16B KO cells was not diminished, as indicated by Western blot of lysates from infected
251 cells examined after a single round of replication (Fig. 6C, rightmost blot). This suggests
252 that the reduced levels of Env seen on the PM and on particles derived from KIF16B KO
253 cells were not due to an Env production defect. To evaluate the significance of the
254 diminished particle incorporation of Env induced by KIF16B KO, we next examined
255 particle infectivity and viral replication. Consistent with the observed reduction of Env on
256 particles, the infectivity of particles released from KIF16B KO cells was consistently
257 reduced (Fig. 6D). We noted that the reduction in Env incorporation shown in Fig. 6C and
258 the reduction in particle infectivity in 6D were consistent but are incomplete, suggesting
259 that although KIF16B alters the level of Env incorporation, it is not absolutely required for
260 incorporation of Env into particles. To determine the significance of this level of Env
261 reduction on viral replication, we infected WT H9 and KIF16B KO cells and measured
262 viral replication in a spreading infection. Infection of KIF16B KO H9 cells resulted in a
263 significant delay in replication and a reduced peak of released virus as compared with
264 WT H9 cells (Fig. 6E). We conclude from these results that the anterograde movement
265 of Env by KIF16B plays a role in Env incorporation and viral replication. Loss of KIF16B
266 results in lower levels of cell surface Env and a corresponding loss of Env incorporation
267 into particles.

268

269 **DISCUSSION**

270 Molecular motor proteins are essential to the normal function of eukaryotic cells. The
271 cytoplasm of cells is dense, crowded with proteins, vesicles, nucleotides, and organelles.

272 Free diffusion of large molecules within the cytoplasm is restricted, and cannot be relied
273 upon to move these cellular materials with the efficiency and accuracy required for proper
274 cell function. Instead, the cell must use specialized molecular motors. These motors –
275 kinesins, dyneins, and myosins – use adenosine triphosphate (ATP) to power movement
276 of cargo along cytoskeletal structures. Kinesins and dyneins utilize microtubule networks
277 as their pathways for transporting cellular cargo. With some exceptions, kinesins move in
278 an anterograde direction along microtubules. Dyneins, in contrast, move in a retrograde
279 direction toward the minus end of microtubules often localized at the microtubule-
280 organizing center (MTOC). Kinesins and dyneins are most commonly structured with an
281 N-terminal motor head that is responsible for powering processive, step-like movement
282 of motor subunits, attached via a middle stalk region to a C-terminal tail composed of light
283 and heavy chains that bind the cellular cargo (20-23) .

284 Viruses hijack host cellular pathways in order to perform essential steps in their
285 lifecycle, including co-opting molecular motor-driven intracellular transport (24-27). HIV-1
286 has been shown to utilize motor proteins at several steps of replication (27, 28). Following
287 entry to a cell, the conical core of HIV-1 has been shown to bind to dynein and to use the
288 KIF5 motor protein to successfully traffic towards the nucleus (29, 30). Depletion of the
289 KIF5B motor prevents nuclear entry and infection of HIV-1 in a CA-dependent manner
290 (31). In studies of outward trafficking of Gag, KIF4 has been shown to directly interact
291 with Gag in both yeast two-hybrid and co-immunoprecipitation assays (32, 33).
292 Additionally, disruption of KIF4 slowed progression of Gag through trafficking
293 intermediates, and depletion of KIF4 increased degradation of Gag that was reversed
294 upon reintroduction of KIF4 (34). However, no motor protein has previously been shown

295 to interact with the HIV-1 Env protein or participate in its trafficking within host cells.
296 Because Env that reaches the cell surface through the secretory pathway is rapidly
297 endocytosed and must subsequently traffic in an anterograde manner to return to the PM
298 for particle incorporation, we hypothesized in this study that HIV-1 would also likely use
299 a kinesin or kinesins for outward trafficking of Env. Several pieces of evidence implicate
300 Rab14 as an important outward trafficking factor for Env. Our group has shown that
301 Rab14 mediates FIP1C-dependent recycling of Env and plays a role in Env incorporation
302 (10). Hoffman and colleagues similarly found that Env colocalizes to Rab14+ endosomal
303 compartments in T cell lines, and unexpectedly found that these compartments shared
304 some characteristics with late endosomes and lysosomes (13). KIF16B is an effector of
305 Rab14-mediated trafficking that binds directly to Rab14 (15). In this study, we
306 demonstrate that KIF16B plays a role in Env trafficking and in the ability of HIV-1 to form
307 fully infectious particles. Similar to other reported cargo of KIF16B such as EGFR, Env
308 colocalized strongly with KIF16B at the periphery of cells. Motor mutant dominant
309 negative KIF16B redistributed Env to a perinuclear position, entirely consistent with what
310 had been seen for EGFR. Video microscopy of pulse-labeled Env expressed on the
311 surface of cells in this study indicated that Env on the PM is endocytosed into KIF16B-
312 positive compartments. In the absence of KIF16B, Env was shifted to the lysosome, and
313 the half-life of Env that had been endocytosed from the PM was significantly reduced.
314 Taken together, these studies strongly suggest that KIF16B mediates anterograde
315 movement of Env and limits the pool of Env that is shunted to the lysosome for
316 degradation. To our knowledge, this is the first evidence for a motor protein contributing
317 to Env trafficking and particle incorporation.

318 Data from this study support the model shown in Fig. 7. According to this model, Env
319 is transported through the secretory pathway to the PM and subsequently endocytosed
320 to the early or recycling compartments, following which Env can be directed in an
321 anterograde fashion by KIF16B or can follow a default pathway leading to fusion with the
322 lysosome (Fig. 7A). In the absence of KIF16B, a larger pool of endocytosed Env is
323 shunted to the lysosome, as indicated by the relative size of the arrows in Fig. 7B. The
324 fraction of the endocytosed pool of Env that is directed to the periphery and is
325 subsequently available for incorporation into particles is diminished in the absence of
326 KIF16B, resulting in diminished particle incorporation, particle infectivity, and reduced
327 replication. Fig. 7 for simplicity does not include other potential trafficking routes of Env,
328 such as retrograde trafficking to the Golgi and the potential for alternative routes for Env
329 to recycle to the PM.

330 Four models for Env incorporation into HIV particles have been proposed by the Freed
331 laboratory (5). Passive incorporation at the PM is not likely to be the correct model in
332 nonpermissive cell types including primary T cells and macrophages, as Env with a full-
333 length CT is excluded in these cell types. This model remains a potential in permissive
334 cell lines that do not require the CT (4). The identification of host factors such as Rab11-
335 FIP1C, Rab14, and KIF16B that influence particle incorporation favors the Gag-Env co-
336 targeting model, whereby Env is directed to specific microdomains on the PM that are
337 enriched in Gag molecules and serve as sites of particle budding. At present there is no
338 evidence favoring an indirect interaction model with an adaptor or linker connecting Gag
339 to Env. The direct Gag-Env interaction model has been supported by two biochemical
340 studies (35, 36), and by evidence that maturation is required before Env can mediate

341 membrane fusion, while CT truncation relieves the constraint on fusion posed by the
342 immature Gag lattice (9, 37, 38). Trimerization of MA has been shown to be required for
343 Env incorporation, while some mutations in MA that result in Env exclusion from particles
344 can be rescued by compensatory mutations at the trimer interface (39, 40). Furthermore,
345 MA trimerization-impaired mutants can be rescued by substitutions that simultaneously
346 restore Env incorporation (41). This has added substantially to the evidence favoring an
347 interaction of the CT with MA in the form of MA trimers, and supports a model whereby
348 the structural integrity of the MA lattice is an important determinant of Env incorporation
349 (41). Results in the present study showing a role for kinesin-mediated trafficking of Env
350 do not negate the importance of structural integrity of the MA lattice for particle
351 incorporation of Env. Trafficking to the site of the developing Gag lattice mediated by host
352 factor interactions with the CT may be a necessary step preceding a direct Gag-Env
353 interaction. We expect that a defect in anterograde trafficking and increase in Env
354 degradation in the lysosome would diminish the delivery of Env to sites of assembly and
355 reduce the potential interaction of Env with the Gag lattice.

356 This study provides new information regarding the half-life of Env trimers following
357 endocytosis from the PM. A prior study employing autoradiographic pulse-labeling of total
358 cellular Env indicated that cellular gp160 and gp120 are degraded over a period of hours,
359 and that inhibition of lysosomal acidification prevents gp160 degradation (42).
360 Degradation of gp160 has been shown to not only occur in the lysosome, but also within
361 the biosynthetic pathway within the ER or Golgi compartments (43, 44). However, these
362 studies labeled all Env populations within the cell, whereas the current study utilized two
363 methods of cell surface pulse-labeling followed by chase periods to measure the half-life

364 of Env trimers that had reached the plasma membrane. We found that endocytosed Env
365 has a half-life of 150-160 minutes, and that the absence of KIF16B promotes much more
366 rapid degradation (57 or 32 minutes, measured by FAP-Env degradation or surface
367 biotinylation, respectively). An important role for lysosomal degradation of endocytosed
368 Env is suggested by the reversal of the enhanced rates of degradation in KIF16B KO cells
369 by Baf-A1. A model in which endocytosed Env is shunted to the lysosome for degradation
370 in the absence of KIF16B is also supported by the increased appearance of Env in
371 lysosomal compartments in KIF16B KO cells.

372 An important caveat for our conclusions is that a complete KIF16B KO resulted in an
373 incomplete reduction of Env incorporation and particle infectivity. Env incorporation and
374 particle infectivity were diminished by approximately 50%. This suggests that kinesins
375 other than KIF16B may also be involved in trafficking Env to the PM, or that there are
376 multiple pathways whereby Env may be recycled to the surface. Indeed, it is known that
377 successful movement of cargo within cells is often accomplished by groups of motors
378 rather than just one (45). Retrograde trafficking of Env from early endosomes to the Golgi
379 may play a role in Env incorporation into particles, as depletion of components of the
380 retromer complex modulated Env distribution and particle incorporation (46). However,
381 the identification of KIF16B as a regulator of Env trafficking and degradation defines
382 another component of the host machinery regulating Env incorporation. Kinesins have
383 been proposed as potential therapeutic targets in some areas of medicine such as cancer
384 and chronic pain (47-49). Although targeting KIF16B function globally would be disruptive
385 to many cell processes, it is possible that a more directed approach disrupting KIF16B-
386 mediated Env trafficking can be developed. In conclusion, we identify KIF16B as an

387 anterograde motor involved in Env trafficking and particle incorporation. Future studies
388 will be needed to fully elucidate the complex pathways taken by Env to reach the site of
389 particle assembly and enable particle incorporation.
390

391 **MATERIALS AND METHODS**

392 **Cells and Plasmids.** HeLa cells were obtained from the American Type Culture
393 Collection (ATCC; CRM-CCL-2). TZM-bl cells were obtained through the NIH AIDS
394 Reagent Program, Division of AIDS, NIAID, NIH, from John C. Kappes, Xiaoyun Wu, and
395 Tranzyme, Inc. The H9 T cell line was obtained from ATCC (HTB-176), and cells were
396 maintained in RPMI medium 1640 supplemented with 10% fetal bovine serum (FBS), 2
397 mM Glutamine, and antibiotics. HeLa and TZM-bl cells were maintained in DMEM
398 (Dulbecco's modified Eagle medium) containing 10% FBS and 2 mM penicillin-
399 streptomycin. pNL4-3 proviral plasmid was obtained through the NIH AIDS Reagent
400 Program, Division of AIDS, NIAID, NIH, from Malcolm Martin. Env expression plasmid
401 pIIINL4Env was a gift kindly provided by Dr. Eric Freed (HIV DRP, NCI, NIH) (6). The
402 Influenza A vaccine strain of A/Brisbane/02/2018 (H1N1) HA sequence was used to
403 construct a human codon-optimized gene which was synthesized and cloned into the
404 BamHI and EcoRI sites of pcDNA3.1+ by GenScript. The SARS-CoV-2 spike gene
405 (Wuhan) was synthesized by Genscript for Dr. Biao He (University of Georgia) and gifted
406 to our lab. The human codon-optimized full length SARS-CoV-2 spike gene was
407 subcloned into the KpnI and BamHI sites of the plasmid pcDNA5TO/Puro. pcDNA5/TO-
408 puro was constructed from backbone pCDNA5/TO (ThermoFisher Scientific) as
409 previously described (50). The EBOV S protein plasmid pcDNA5/TO-puro EBOV GP has

410 been previously described (51). Plasmid pcDNA5/TO JR-FLoptgp160 expresses a
411 codon-optimized JR-FL *env* gene in the pcDNA5/TO vector backbone (Thermo Fisher
412 Scientific, Waltham, MA) as previously described (12). Overlap-extension PCR was used
413 to create novel Xho1 and Pst1 sites within the exposed portion of the V2 loop of JR-FL.
414 The fluorogen-activated peptide (FAP) sequence from pMFAP-alpha2 (Spectragenetics,
415 Pittsburgh, PA) was PCR amplified as an Xho1-Pst1 fragment and ligated into
416 pcDNA5/TO JR-FLoptgp160, placing the FAP peptide in-frame within the V2 loop. A
417 complete cloning schema with primers is available upon request. The WT KIF16B-YFP
418 and dominant KIF16B-S109A-YFP were kindly provided by Sebastian Hoepfner (14).
419 Expression plasmids for Flag-KIF1Bβ and Flag- KIF1Bβ Q98L were kindly provided
420 Susanne Schlisio and described in Fell et. al. 2017 (18).

421 **Viral infectivity and multi-round replication assays.** H9 T cells were infected with
422 VSV G-pseudotyped NL4-3 virus at an MOI of 0.2. Cells and supernatants were harvested
423 4-5 days after infection for analysis by Western blotting, p24 antigen quantitation, and
424 infectivity assays. Infectivity of cell culture supernatants was measured using TZM-bl
425 indicator cells following p24 normalization as previously described (52). Replications
426 assays were performed by taking aliquots of the supernatant after infection every 3 days
427 for 21 days. Supernatant was then used in a p24 ELISA assay to graph the amount of
428 virus produced over the course of viral growth and replication. Murine anti-p24 capture
429 antibody 183-H12-5C (CA183) was obtained from Bruce Chesebro and Kathy Wehrly
430 through the NIH AIDS Research and Reference Reagent Program, and the p24 ELISA
431 assay was performed as previously described (53).

432 **Western blotting, antibodies, and immunostaining.** For analysis of viral protein
433 content, viruses were pelleted from cell culture supernatants through a 20% sucrose
434 cushion at 35,000 × g for 3 h at 4°C; cells were harvested and pelleted at 400 × g. Virus
435 pellets and cell lysates were dissolved in radioimmunoprecipitation assay (RIPA) buffer
436 (Thermo Scientific) containing protease inhibitors. Cell lysates for blotting KIF16B were
437 prepared with a hypotonic lysis buffer consisting of 10mM Hepes, 1.5mM $MgCL_2$, 10 mM
438 KCl in PBS on ice for 15 minutes, vortexed with 10% IGEPAL CA630 (Sigma) to break
439 open cells, and then centrifuged to pellet out nuclei. Virus pellets and cell lysates were
440 separated on 4 to 12% polyacrylamide gels, transferred to nitrocellulose, and subjected
441 to Western blotting using antibodies outlined below. Goat polyclonal antibody AHP2204,
442 from Bio-Rad AbD Serotec (Oxford, UK)(D7324), was used for detecting HIV-1 gp120 for
443 Western blotting. Recombinant human monoclonal antibody 2F5 from Polymun scientific
444 (Klosterneuburg, Austria) was used to detect HIV-1 gp41 in Western blots. Actin was
445 detected with Invitrogen Actin antibody ACTN05. KIF16B antibody used was polycolonal
446 mouse from Abnova (H00055614-B01P). Mouse anti-p24 monoclonal CA-183 (provided
447 by Bruce Chesebro and Kathy Wehrly through the NIH AIDS Research and Reference
448 Reagent Program) was used to detect p24 and $Pr55^{Gag}$ in Western blotting and for
449 enzyme-linked immunosorbent assay (ELISA) to measure HIV-1 Gag in virus-containing
450 culture supernatant and virus pellets; the capture ELISA was performed as previously
451 described (54). IRDye goat anti-mouse, IRDye rabbit anti-goat, and IRDye goat anti-rabbit
452 secondary antibodies from LiCor Biosciences (Lincoln, NE) were used for Western
453 blotting. All blots were acquired and analyzed using the LiCor Odyssey infrared detection
454 system. The following antibodies were utilized in immunofluorescence assays: human

455 anti-gp120 antibody IgG1 2G12 from Polymun scientific (A002), monoclonal ANTI-
456 FLAG® antibody produced in rabbit from Sigma-Aldrich (F2555), rabbit polyclonal anti-
457 HA1 antibody from Sino Biological (Beijing, China) (11692-T54), mouse monoclonal
458 SARS-CoV / SARS-CoV-2 (COVID-19) spike antibody from Genetex (Irvine, CA) (1A9),
459 mouse anti- EBOV GP monoclonal antibody 4F3 from IBT Bioservices (Rockville, MD),
460 anti-LAMP1 mouse monoclonal antibody from BD Biosciences (Franklin Lakes, NJ)
461 (H4A3).

462 **Env degradation assays.** In order to determine degradation rates of Env
463 microscopically using our FAP-tagged Env, we plated 100k HeLa WT or KIF16B KO HeLa
464 cells in wells of Ibidi 4 well μ-Slide plate (Ibidi) and then transfected overnight with the
465 FAP-Env construct. In one of the KO cell wells, 100μM concentration of Bafilomycin A1
466 (Baf-A1, Invivogen) was employed while the WT and other KO cell wells received an
467 equal amount of DMSO. Three hours later, live cell imaging was conducted following a
468 10 min pulse label incubation with FAP reagent αRED-np1 (Spectragenetics) in 5% CO_2
469 at 37°C chamber on Widefield Nikon Ti2 inverted SpectraX (Cincinnati Children's
470 Confocal Core). Data from these movies was extracted on Volocity imaging software
471 (Quorum Technologies) to acquire the signal intensity of each ROI drawn around
472 individual cells analyzed in the field of view over the time course. The averaged
473 normalized signal intensity was then calculated using the method outlined in Alber et. al.
474 to attain the degradation curve and half-life of the FAP-tagged Env protein (55). For
475 protein analysis of Env degradation by Western blotting, we plated 1.75 million WT or
476 KIF16B KO HeLa cells in 10cm dishes (5 for WT, 10 for KO). The next morning, 3ug of
477 pIII-Env and 250 ng of psv72-Tat protein were cotransfected into each plate. Following

478 24 hours of incubation, 100μM Baf-A1 was added to 5 of the KO dishes, while the other
479 KO and WT dishes received an equal amount of DMSO. Three hours later a 1 mM solution
480 of biotin/PBS was applied to the cells and allowed to label surface proteins for 15 min.
481 This labeling reaction was quenched with 1x TBS solution for 5 min. Cells were then
482 washed with PBS and returned to normal media. Cell plates were then put on ice and in
483 a 4°C cold room to stop endocytosis at 0, 30, 60, 90, 120 min after biotin labeling and
484 were then subsequently scrapped and harvested for cell lysates in RIPA buffer. Cell
485 lysates were then IP overnight with 60μL of Pierce™ High Capacity NeutrAvidin™
486 Agarose (Thermo-Fischer). Beads were then collected in Pierce™ Spin Columns
487 (Thermo-Fischer) and protein was then eluted off the beads at 95°C in 1x Laemli buffer
488 with reducing agent. After 2000 x g spin for 3 min equal amounts of elution were run for
489 each time point on a 4-12% SDS-Page gel and then analyzed by immunoblotting for
490 gp120.

491 **Image acquisition and analysis.** HeLa cells were plated in MatTek 35mm poly–d-
492 lysine-treated dishes (Brooke Knapp MatTek) overnight and then were then transfected
493 with the indicated constructs using jetPRIME (Polyplus) per manufacturer's instructions.
494 After a 24 h incubation, cells were rinsed with phosphate-buffered saline (PBS) three
495 times and fixed in 4% paraformaldehyde for 10 min at room temperature. Cells were
496 washed with PBS three times with mild agitation after fixation, and then permeabilized for
497 10 min with 0.2% Triton X-100, followed by washing with PBS. Dako blocking solution
498 was applied to cells for 30 min under gentle shaking conditions. Cells were then incubated
499 with the appropriate primary antibody detailed above diluted in Dako (Agilent) antibody
500 diluent to 1:500. Species appropriate Alexa-flour (Thermo-Fischer) secondary antibody

501 was diluted in Dako antibody diluent to 1:1,000. Images were acquired on a widefield
502 DeltaVision Elite High Resolution microscope (GE Healthcare). Percent of total Env signal
503 at the periphery of cells was calculated using measurements from Volocity 6.5.1 imaging
504 analysis software. Briefly, regions of interest were drawn around the entire cell, around
505 30% of the distance from the edge of the cell signal to the nucleus (inner 70% of total cell
506 area), and around the nucleus. Peripheral signal was calculated by subtracting the middle
507 two regions from the sum of signal from the total cell region, giving a percentage of
508 peripheral signal as all signal in the last 30% of the cell body towards the edge.
509 Quantitation of colocalization was performed using Volocity software features by
510 derivation of Pearson's correlation coefficient after manual thresholding.

511 **Flow cytometry for HIV-1 Env expression on cell surface.** For cell surface staining,
512 approximately 5 million H9 cells were infected overnight with 1000 ng p24 of VSV-G-
513 pseudotyped NL4.3. The next day, cells were washed once with PBS and plated in a six
514 well plate in RPMI for 48 hours. Infected cells were stained for viability with zombie violet
515 dye (BioLegend) diluted 1:500 in PBS, followed by fixation with 4% paraformaldehyde.
516 Cells were blocked with Dako protein block then stained for cell surface Env with 2G12
517 anti-gp120 directly conjugated to APC (Abcam, ab201807) and diluted 1:100 in Dako
518 antibody diluent (10ug/mL final concentration) for 2 hours. 2G12 was washed out twice
519 with PBS followed by permeabilization with 0.2% triton-X 100. Lastly, cells were stained
520 for total infected cells using p24 antibody, KC-57 FITC diluted 1:100 in Dako antibody
521 diluent. Cells were washed twice with PBS then resuspended in MACS (Miltenyi Biotec)
522 buffer and analyzed using the BD FACS Canto II.

523 **CRISPR KO strategy.** CRISPR-Cas9 technology was used to knockout KIF16B in
524 both HeLa and H9 cell lines. Using the Crispor.tefor.net open access website and
525 algorithm designed to find areas of the genome to target with guide RNAs (gRNA), we
526 targeted Exon 13 of KIF16B using sequence from NCBI (Gene ID 55614, Assebmly
527 GCF_000001405.40, Chr 20, location NC_000020.11) and found the stretch of DNA with
528 the highest score to target for deletion being CTCACGGATAAGTTTGACGT. We ordered
529 sense (CACCGCTCACGGATAAGTTTGACGT) and anti-sense
530 (AAACACGTCAAACTTATCCGTGAGC) gRNA oligos + PAM sequence from Integrated
531 DNA Technologies (IDT) to clone into the lentiCRISPR v2 that was a gift from Feng Zhang
532 (Addgene plasmid # 52961 ; http://n2t.net/addgene:52961 ; RRID:Addgene_52961) using
533 the target guide sequence protocol from Sanjana Lab
534 (http://sanjanalab.org/library/protocol_lentiOligo.pdf) (56) After transformation of MAX
535 Efficiency™ Stbl2™ Competent Cells (Thermo-Fischer) and DNA harvest, we packaged
536 the plasmid into a lentivirus using sPAX2 and PMGD2 and transduced our HeLa and H9
537 cell lines. Puromycin selection and limiting dilution were used to obtain clones knocked
538 out for KIF16B (Fig. S1).
539

540 **ACKNOWLEDGMENTS**

541 This work was supported by 5R01AI150486-24
542 The funders had no role in study design, data collection and interpretation, or the decision
543 to submit the work for publication.
544 Flow cytometry was performed using the Cincinnati Children's Hospital Medical Center
545 (CCHMC) Flow Cytometry Core. Live cell imaging of was conducted in the Confocal

546 Imaging Center at CCHMC. DNA sequencing was performed at the DNA Sequencing
547 core at CCHMC.

548

549 **REFERENCES**

550 1. Egan MA, Carruth LM, Rowell JF, Yu X, Siliciano RF. 1996. Human
551 immunodeficiency virus type 1 envelope protein endocytosis mediated by a
552 highly conserved intrinsic internalization signal in the cytoplasmic domain of gp41
553 is suppressed in the presence of the Pr55gag precursor protein. J Virol 70:6547-
554 56.
555 2. Ohno H, Aguilar RC, Fournier MC, Hennecke S, Cosson P, Bonifacino JS. 1997.
556 Interaction of endocytic signals from the HIV-1 envelope glycoprotein complex
557 with members of the adaptor medium chain family. Virology 238:305-15.
558 3. Rowell JF, Stanhope PE, Siliciano RF. 1995. Endocytosis of endogenously
559 synthesized HIV-1 envelope protein. Mechanism and role in processing for
560 association with class II MHC. J Immunol 155:473-88.
561 4. Anokhin B, Spearman P. 2022. Viral and Host Factors Regulating HIV-1
562 Envelope Protein Trafficking and Particle Incorporation. Viruses 14.
563 5. Checkley MA, Luttge BG, Freed EO. 2011. HIV-1 envelope glycoprotein
564 biosynthesis, trafficking, and incorporation. J Mol Biol 410:582-608.
565 6. Murakami T, Freed EO. 2000. The long cytoplasmic tail of gp41 is required in a
566 cell type-dependent manner for HIV-1 envelope glycoprotein incorporation into
567 virions. Proceedings of the National Academy of Sciences 97:343-348.
568 7. Akari H, Fukumori T, Adachi A. 2000. Cell-dependent requirement of human
569 immunodeficiency virus type 1 gp41 cytoplasmic tail for Env incorporation into
570 virions. J Virol 74:4891-3.
571 8. Dubay JW, Roberts SJ, Hahn BH, Hunter E. 1992. Truncation of the human
572 immunodeficiency virus type 1 transmembrane glycoprotein cytoplasmic domain
573 blocks virus infectivity. J Virol 66:6616-25.
574 9. Jiang J, Aiken C. 2007. Maturation-dependent human immunodeficiency virus
575 type 1 particle fusion requires a carboxyl-terminal region of the gp41 cytoplasmic
576 tail. J Virol 81:9999-10008.
577 10. Qi M, Williams JA, Chu H, Chen X, Wang J-J, Ding L, Akhirome E, Wen X,
578 Lapierre LA, Goldenring JR, Spearman P. 2013. Rab11-FIP1C and Rab14 Direct
579 Plasma Membrane Sorting and Particle Incorporation of the HIV-1 Envelope
580 Glycoprotein Complex. 9:e1003278.
581 11. Qi M, Chu H, Chen X, Choi J, Wen X, Hammonds J, Ding L, Hunter E, Spearman
582 P. 2015. A tyrosine-based motif in the HIV-1 envelope glycoprotein tail mediates
583 cell-type– and Rab11-FIP1C–dependent incorporation into virions. 112:7575-
584 7580.
585 12. Kirschman J, Qi M, Ding L, Hammonds J, Dienger-Stambaugh K, Wang J-J,
586 Lapierre LA, Goldenring JR, Spearman P. 2017. HIV-1 Envelope Glycoprotein
587 Trafficking through the Endosomal Recycling Compartment Is Required for
588 Particle Incorporation. Journal of Virology 92.
589 13. Hoffman HK, Aguilar RS, Clark AR, Groves NS, Pezeshkian N, Bruns MM, van
590 Engelenburg SB. 2022. Endocytosed HIV-1 Envelope Glycoprotein Traffics to
591 Rab14(+) Late Endosomes and Lysosomes to Regulate Surface Levels in T-Cell
592 Lines. J Virol 96:e0076722.

14. Hoepfner S, Severin F, Cabezas A, Habermann B, Runge A, Gillooly D, Stenmark H, Zerial M. 2005. Modulation of Receptor Recycling and Degradation by the Endosomal Kinesin KIF16B. Cell 121:437-450.
15. Ueno H, Huang X, Tanaka Y, Hirokawa N. 2011. KIF16B/Rab14 Molecular Motor Complex Is Critical for Early Embryonic Development by Transporting FGF Receptor. 20:60-71.
16. Weimershaus M, Mauvais FX, Saveanu L, Adiko C, Babdor J, Abramova A, Montealegre S, Lawand M, Evnouchidou I, Huber KJ, Chadt A, Zwick M, Vargas P, Dussiot M, Lennon-Dumenil AM, Brocker T, Al-Hasani H, van Endert P. 2018. Innate Immune Signals Induce Anterograde Endosome Transport Promoting MHC Class I Cross-Presentation. Cell Rep 24:3568-3581.
17. Perez Bay AE, Schreiner R, Mazzoni F, Carvajal-Gonzalez JM, Gravotta D, Perret E, Lehmann Mantaras G, Zhu YS, Rodriguez-Boulan EJ. 2013. The kinesin KIF16B mediates apical transcytosis of transferrin receptor in AP-1B-deficient epithelia. EMBO J 32:2125-39.
18. Fell SM, Li S, Wallis K, Kock A, Surova O, Rraklli V, Höfig CS, Li W, Mittag J, Henriksson MA, Kenchappa RS, Holmberg J, Kogner P, Schlisio S. 2017. Neuroblast differentiation during development and in neuroblastoma requires KIF1Bβ-mediated transport of TRKA. Genes & Development 31:1036-1053.
19. Szent-Gyorgyi C, Schmidt BF, Creeger Y, Fisher GW, Zakel KL, Adler S, Fitzpatrick JA, Woolford CA, Yan Q, Vasilev KV, Berget PB, Bruchez MP, Jarvik JW, Waggoner A. 2008. Fluorogen-activating single-chain antibodies for imaging cell surface proteins. Nat Biotechnol 26:235-40.
20. Hirokawa N, Noda Y, Tanaka Y, Niwa S. 2009. Kinesin superfamily motor proteins and intracellular transport, vol 10, p 682-696.
21. Verhey KJ, Hammond JW. 2009. Traffic control: Regulation of kinesin motors, vol 10, p 765-777.
22. Gennerich A, Vale RD. 2009. Walking the walk: how kinesin and dynein coordinate their steps, vol 21, p 59-67. NIH Public Access.
23. Kardon JR, Vale RD. 2009. Regulators of the cytoplasmic dynein motor, vol 10, p 854-865. NIH Public Access.
24. Greber UF, Way M. 2006. A superhighway to virus infection, vol 124, p 741-754.
25. Döhner K, Nagel CH, Sodeik B. 2005. Viral stop-and-go along microtubules: Taking a ride with dynein and kinesins, vol 13, p 320-327. Elsevier.
26. Radtke K, Döhner K, Sodeik B. 2006. Viral interactions with the cytoskeleton: A hitchhiker's guide to the cell, vol 8, p 387-400.
27. Ward BM. 2011. The taking of the cytoskeleton one two three: How viruses utilize the cytoskeleton during egress, vol 411, p 244-250. Elsevier.
28. Brandenburg B, Zhuang X. 2007. Virus trafficking - Learning from single-virus tracking, vol 5, p 197-208. NIH Public Access.
29. Carnes SK, Zhou J, Aiken C. 2018. HIV-1 Engages a Dynein-Dynactin-BICD2 Complex for Infection and Transport to the Nucleus. Journal of Virology 92.
30. Malikov V, da Silva ES, Jovasevic V, Bennett G, de Souza Aranha Vieira DA, Schulte B, Diaz-Griffero F, Walsh D, Naghavi MH. 2015. HIV-1 capsids bind and exploit the kinesin-1 adaptor FEZ1 for inward movement to the nucleus. Nature Communications 6:6660-6660.

639 31. Dharan A, Talley S, Tripathi A, Mamede JI, Majetschak M, Hope TJ, Campbell
640 EM. 2016. KIF5B and Nup358 Cooperatively Mediate the Nuclear Import of HIV-
641 1 during Infection. PLoS Pathogens 12.
642 32. Gaudin RL, Cunha De Alencar B, Arhel N, Benaroch P. 2013. HIV trafficking in
643 host cells: motors wanted! Trends in Cell Biology 23.
644 33. Tang Y, Winkler U, Freed EO, Torrey TA, Kim W, Li H, Goff SP, Morse HC.
645 1999. Cellular Motor Protein KIF-4 Associates with Retroviral Gag. Journal of
646 Virology 73:10508-10513.
647 34. Martinez NW, Xue X, Berro RG, Kreitzer G, Resh MD. 2008. Kinesin KIF4
648 Regulates Intracellular Trafficking and Stability of the Human Immunodeficiency
649 Virus Type 1 Gag Polyprotein. Journal of Virology 82:9937-9950.
650 35. Alfadhli A, Staubus AO, Tedbury PR, Novikova M, Freed EO, Barklis E. 2019.
651 Analysis of HIV-1 Matrix-Envelope Cytoplasmic Tail Interactions. J Virol 93.
652 36. Cosson P. 1996. Direct interaction between the envelope and matrix proteins of
653 HIV-1. EMBO J 15:5783-8.
654 37. Wyma DJ, Jiang J, Shi J, Zhou J, Lineberger JE, Miller MD, Aiken C. 2004.
655 Coupling of human immunodeficiency virus type 1 fusion to virion maturation: a
656 novel role of the gp41 cytoplasmic tail. J Virol 78:3429-35.
657 38. Murakami T, Ablan S, Freed EO, Tanaka Y. 2004. Regulation of human
658 immunodeficiency virus type 1 Env-mediated membrane fusion by viral protease
659 activity. J Virol 78:1026-31.
660 39. Tedbury PR, Novikova M, Ablan SD, Freed EO. 2016. Biochemical evidence of a
661 role for matrix trimerization in HIV-1 envelope glycoprotein incorporation. Proc
662 Natl Acad Sci U S A 113:E182-90.
663 40. Tedbury PR, Mercredi PY, Gaines CR, Summers MF, Freed EO. 2015.
664 Elucidating the mechanism by which compensatory mutations rescue an HIV-1
665 matrix mutant defective for gag membrane targeting and envelope glycoprotein
666 incorporation. J Mol Biol 427:1413-1427.
667 41. Tedbury PR, Novikova M, Alfadhli A, Hikichi Y, Kagiampakis I, KewalRamani VN,
668 Barklis E, Freed EO. 2019. HIV-1 Matrix Trimerization-Impaired Mutants Are
669 Rescued by Matrix Substitutions That Enhance Envelope Glycoprotein
670 Incorporation. J Virol 94.
671 42. Willey RL, Bonifacino JS, Potts BJ, Martin MA, Klausner RD. 1988. Biosynthesis,
672 cleavage, and degradation of the human immunodeficiency virus 1 envelope
673 glycoprotein gp160. Proc Natl Acad Sci U S A 85:9580-4.
674 43. Courageot J, Fenouillet E, Bastiani P, Miquelis R. 1999. Intracellular degradation
675 of the HIV-1 envelope glycoprotein. Evidence for, and some characteristics of, an
676 endoplasmic reticulum degradation pathway. Eur J Biochem 260:482-9.
677 44. Kimura T, Nishikawa M, Fujisawa J. 1996. Uncleaved env gp160 of human
678 immunodeficiency virus type 1 is degraded within the Golgi apparatus but not
679 lysosomes in COS-1 cells. FEBS Lett 390:15-20.
680 45. Gross SP, Vershinin M, George. 2007. Cargo Transport: Two Motors Are
681 Sometimes Better Than One. Current Biology 17:R478-R486.
682 46. Groppelli E, Len AC, Granger LA, Jolly C. 2014. Retromer regulates HIV-1
683 envelope glycoprotein trafficking and incorporation into virions. PLoS Pathog
684 10:e1004518.

685 47. Shantanu PA, Sharma D, Sharma M, Vaidya S, Sharma K, Kalia K, Tao YX,
686 Shard A, Tiwari V. 2019. Kinesins: Motor Proteins as Novel Target for the
687 Treatment of Chronic Pain. Mol Neurobiol 56:3854-3864.
688 48. Huszar D, Theoclitou ME, Skolnik J, Herbst R. 2009. Kinesin motor proteins as
689 targets for cancer therapy. Cancer Metastasis Rev 28:197-208.
690 49. Liu X, Gong H, Huang K. 2013. Oncogenic role of kinesin proteins and targeting
691 kinesin therapy. Cancer Science 104:651-656.
692 50. Singh K, Marasini B, Chen X, Ding L, Wang JJ, Xiao P, Villinger F, Spearman P.
693 2020. A Bivalent, Spherical Virus-Like Particle Vaccine Enhances Breadth of
694 Immune Responses against Pathogenic Ebola Viruses in Rhesus Macaques. J
695 Virol 94.
696 51. Singh K, Marasini B, Chen X, Spearman P. 2018. A novel Ebola virus antibody-
697 dependent cell-mediated cytotoxicity (Ebola ADCC) assay. Journal of
698 Immunological Methods 460:10-16.
699 52. Hammonds J, Chen X, Fouts T, DeVico A, Montefiori D, Spearman P. 2005.
700 Induction of neutralizing antibodies against human immunodeficiency virus type 1
701 primary isolates by Gag-Env pseudovirion immunization. J Virol 79:14804-14.
702 53. Rai MA, Hammonds J, Pujato M, Mayhew C, Roskin K, Spearman P. 2020.
703 Comparative analysis of human microglial models for studies of HIV replication
704 and pathogenesis. Retrovirology 17:35.
705 54. Hammonds JE, Beeman N, Ding L, Takushi S, Francis AC, Wang JJ, Melikyan
706 GB, Spearman P. 2017. Siglec-1 initiates formation of the virus-containing
707 compartment and enhances macrophage-to-T cell transmission of HIV-1. PLoS
708 Pathog 13:e1006181.
709 55. Alber AB, Suter DM. 2018. Single-Cell Quantification of Protein Degradation
710 Rates by Time-Lapse Fluorescence Microscopy in Adherent Cell Culture. J Vis
711 Exp doi:10.3791/56604.
712 56. Sanjana NE, Shalem O, Zhang F. 2014. Improved vectors and genome-wide
713 libraries for CRISPR screening. Nat Methods 11:783-784.

714

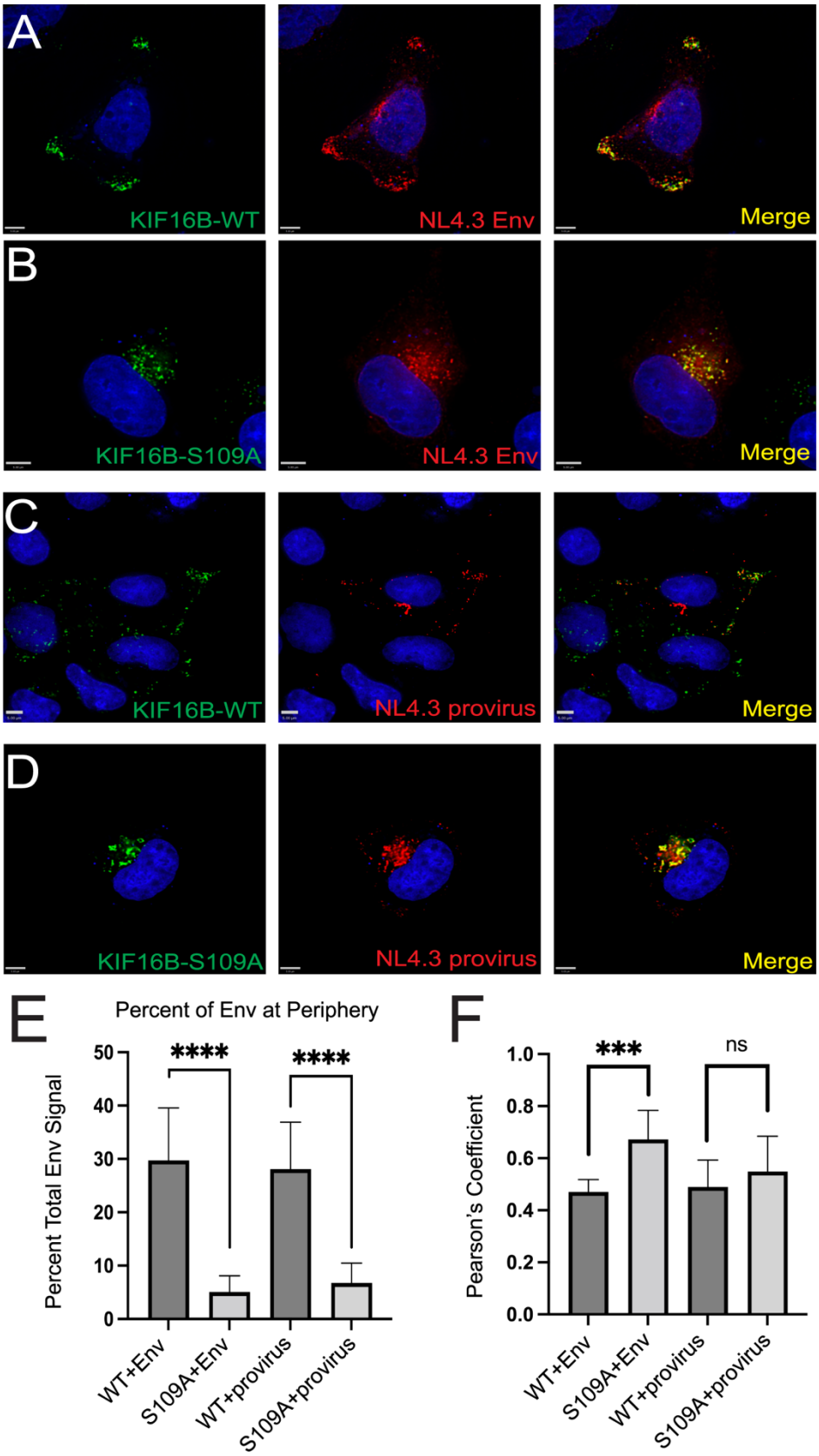
A
KIF16B-WT
NL4.3 Env
Merge
B
KIF16B-S109A
NL4.3 Env
Merge
C
KIF16B-WT
NL4.3 provirus
Merge
D
KIF16B-S109A
NL4.3 provirus
Merge
E
Percent of Env at Periphery
Percent Total Env Signal
50
40
30
20
10
0
****
****
WT+Env
S109A+Env
WT+provirus
S109A+provirus
F
Pearson's Coefficient
1.0
0.8
0.6
0.4
0.2
0.0
***
ns
WT+Env
S109A+Env
WT+provirus
S109A+provirus

715

716 **FIG 1** Env localizes to KIF16B-positive compartments and is redistributed by dominant-
717 negative KIF16B. (A) Subcellular distribution of NL4-3 Env when coexpressed with
718 KIF16B-WT-YFP. Cells were fixed and immunolabeled with human neutralizing antibody
719 2G12 to stain HIV-1 gp120. Green, KIF16B; red, Env; rightmost image, overlay. (B)
720 Distribution of NL4-3 Env when coexpressed with dominant KIF16B-S109A-YFP. Staining
721 is as described for panel A. (C and D) Coexpression of proviral NL4-3 with WT and
722 dominant-negative KIF16B, respectively. Staining for Env as described from A, B. (E)
723 Percent of Env signal at periphery of cells observed for each combination of coexpression
724 shown in A-D. Signal at the periphery was the sum all Env signal within 30% of the
725 distance from edge of cell to the nucleus. Results are shown as means ± SD from a total
726 of 10 representative images. ns = not significant; ***, $P < 0.0008$; ****, $P < 0.0001$. P values
727 were calculated using the Student's unpaired t test using GraphPad Prism 9. (F) The
728 degree of colocalization between KIF16B constructs and Env was measured by
729 Pearson's correlation coefficient equation using Volocity 6.5.1 software after thresholding.
730 Bars represent 5 μm.

731

732

733

734

735

736

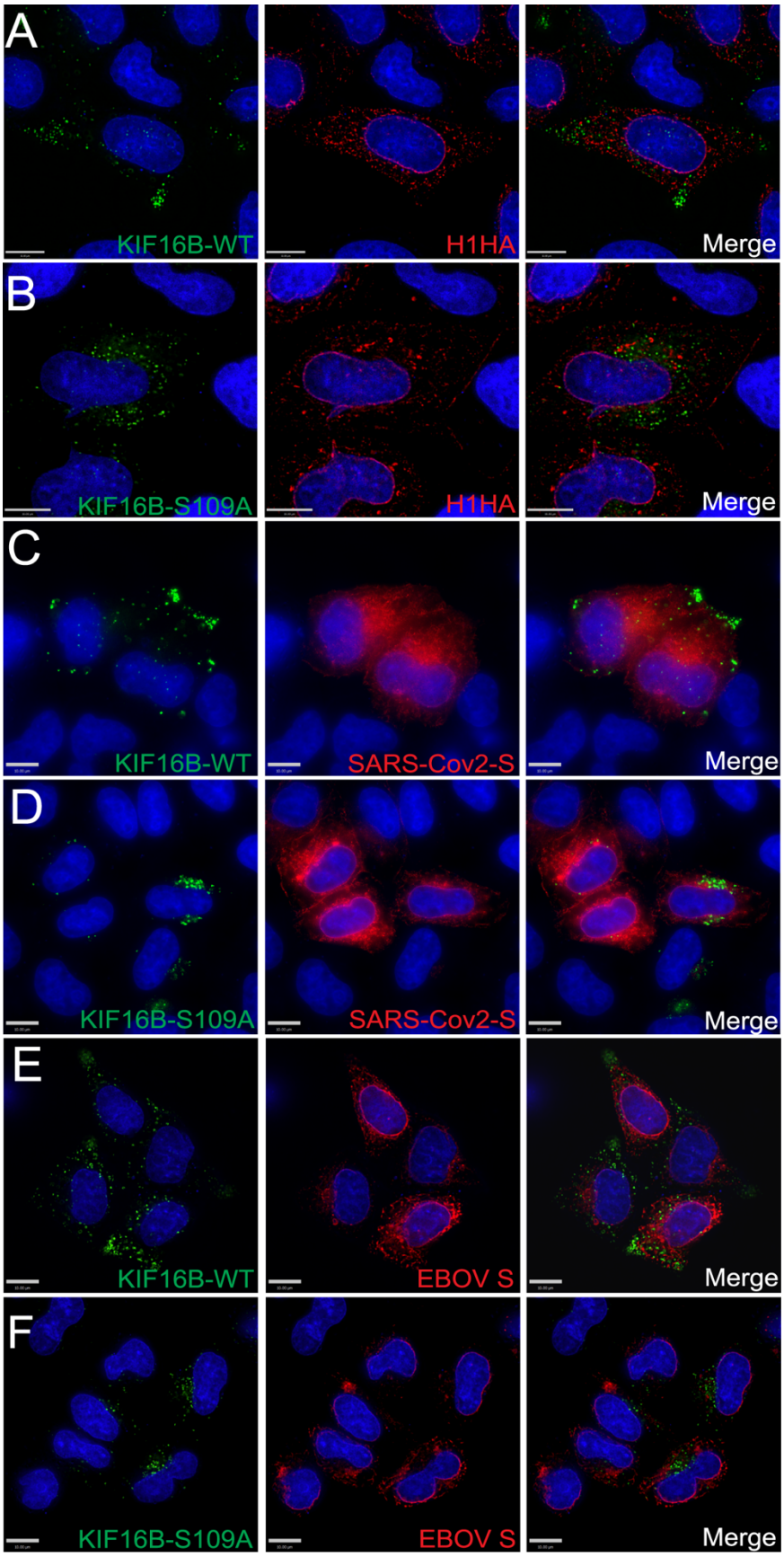
A
KIF16B-WT
H1HA
Merge
B
KIF16B-S109A
H1HA
Merge
C
KIF16B-WT
SARS-Cov2-S
Merge
D
KIF16B-S109A
SARS-Cov2-S
Merge
E
KIF16B-WT
EBOV S
Merge
F
KIF16B-S109A
EBOV S
Merge

737

738 **FIG 2** KIF16B and Env colocalization is not generalized to other viral envelope
739 glycoproteins. (A, B) Influenza HA glycoprotein was coexpressed with KIF16B-WT-YFP
740 and KIF16B-S109A-YFP, respectively. Cells were fixed and immunolabeled with 11692-
741 T54 antibody to stain HA. Green, KIF16B; red, HA; rightmost image, overlay. (C, D)
742 SARS-Cov2-S protein was coexpressed with WT and dominant negative KIF16B,
743 respectively. Cells were fixed and immunolabeled with 1A9 to stain spike. Green, KIF16B;
744 red, SARS-Cov2-S; rightmost image, overlay. (E, F) Coexpression of KIF16B-WT-YFP or
745 KIF16B-S109A-YFP with Ebola GP. Cells were fixed and immunostained with 4F3
746 antibody specific to EBOV GP. Green, KIF16B; red, EBOV GP; rightmost image, overlay.
747 Bars represent 10 μm.

748

749

750

751

752

753

754

755

756

757

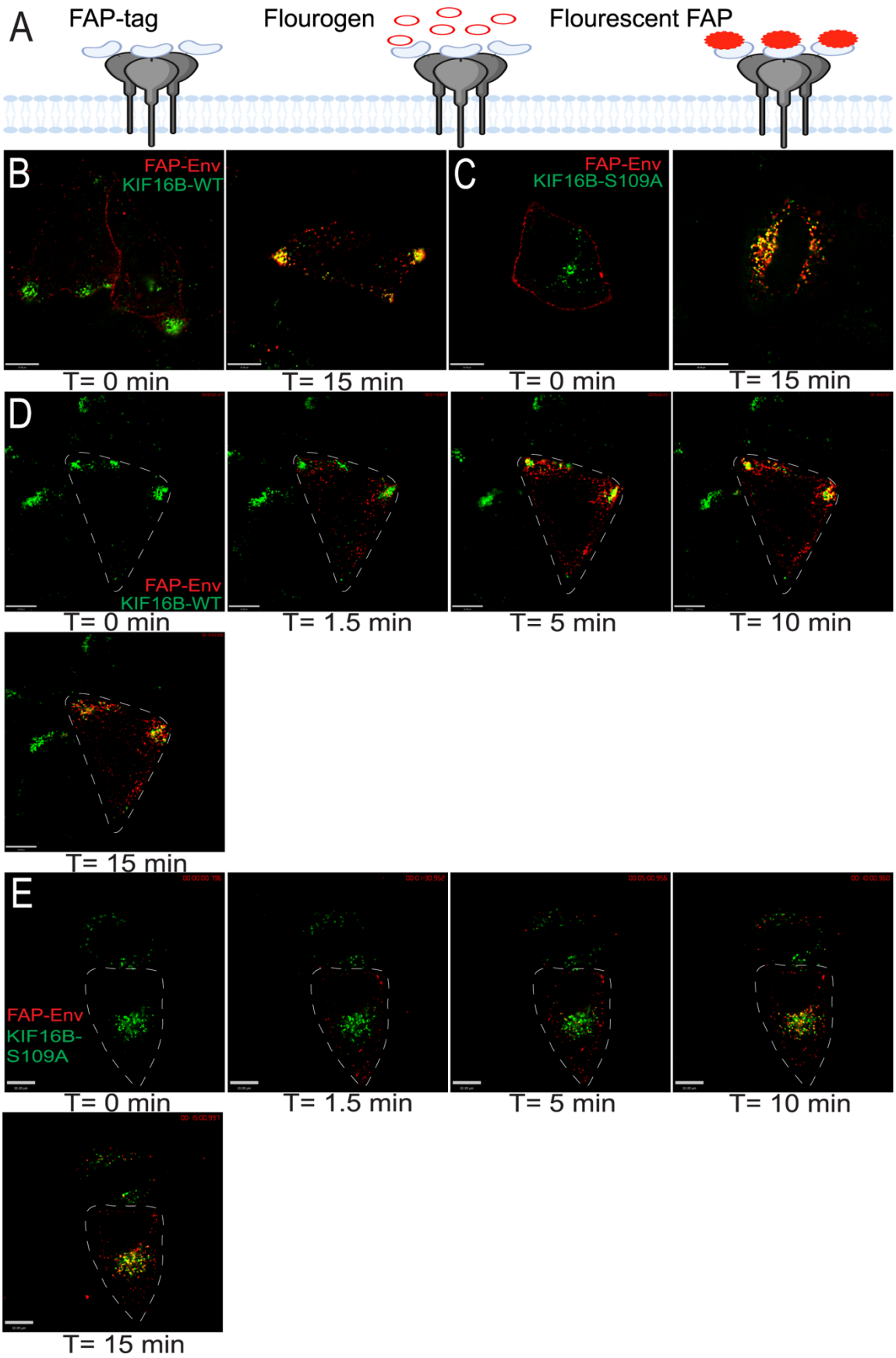
A
FAP-tag
Flourogen
Flourescent FAP
B
FAP-Env
KIF16B-WT
T= 0 min
T= 15 min
C
FAP-Env
KIF16B-S109A
T= 0 min
T= 15 min
D
FAP-Env
KIF16B-WT
T= 0 min
T= 1.5 min
T= 5 min
T= 10 min
T= 15 min
E
FAP-Env
KIF16B-
S109A
T= 0 min
T= 1.5 min
T= 5 min
T= 10 min
T= 15 min

758

759 **FIG 3** Env on the plasma membrane is endocytosed into KIF16B positive compartments.
760 (A) FAP-Env construct shown as cartoon diagram. The FAP-tag was placed on the V2
761 loop of the Env ectodomain. This tag is inherently non-fluorescent on the far left. In the
762 middle, the addition of a non-permeable dye is shown. On the far right, the FAP-tag
763 becomes fluorescent, allowing visualization of a pulsed population of surface Env. (B)
764 FAP-Env coexpressed with KIF16B- WT-YFP in HeLa cells. Left image, FAP-Env is pulse
765 labeled for 10 min on ice. Cells were then fixed and imaged immediately to show
766 population of Env on plasma membrane surface. Right image, cells were pulsed as before
767 and then were returned to 37°C incubator for 15 min to allow internalization, then fixed
768 and imaged to show FAP-Env endocytosed into KIF16B-positive compartments. (C) FAP-
769 Env construct co-expressed with KIF16B-S109A-YFP in HeLa cells. Left image is FAP-
770 Env collecting on surface as before. Right image is cell shown after 15 min of
771 internalization as before. (D, E) Frames from live cell imaging video of FAP-Env
772 coexpressed with KIF16B-WT-YFP and KIF16B-S109A-YFP, respectively. Time T= 0 min
773 shows cell before pulse. Subsequent time points show FAP-Env collecting in KIF16B-
774 positive compartments. Dotted lines are a visual aid to represent periphery of cell body.
775 Bars represent 10 μm.

776

777

778

779

780

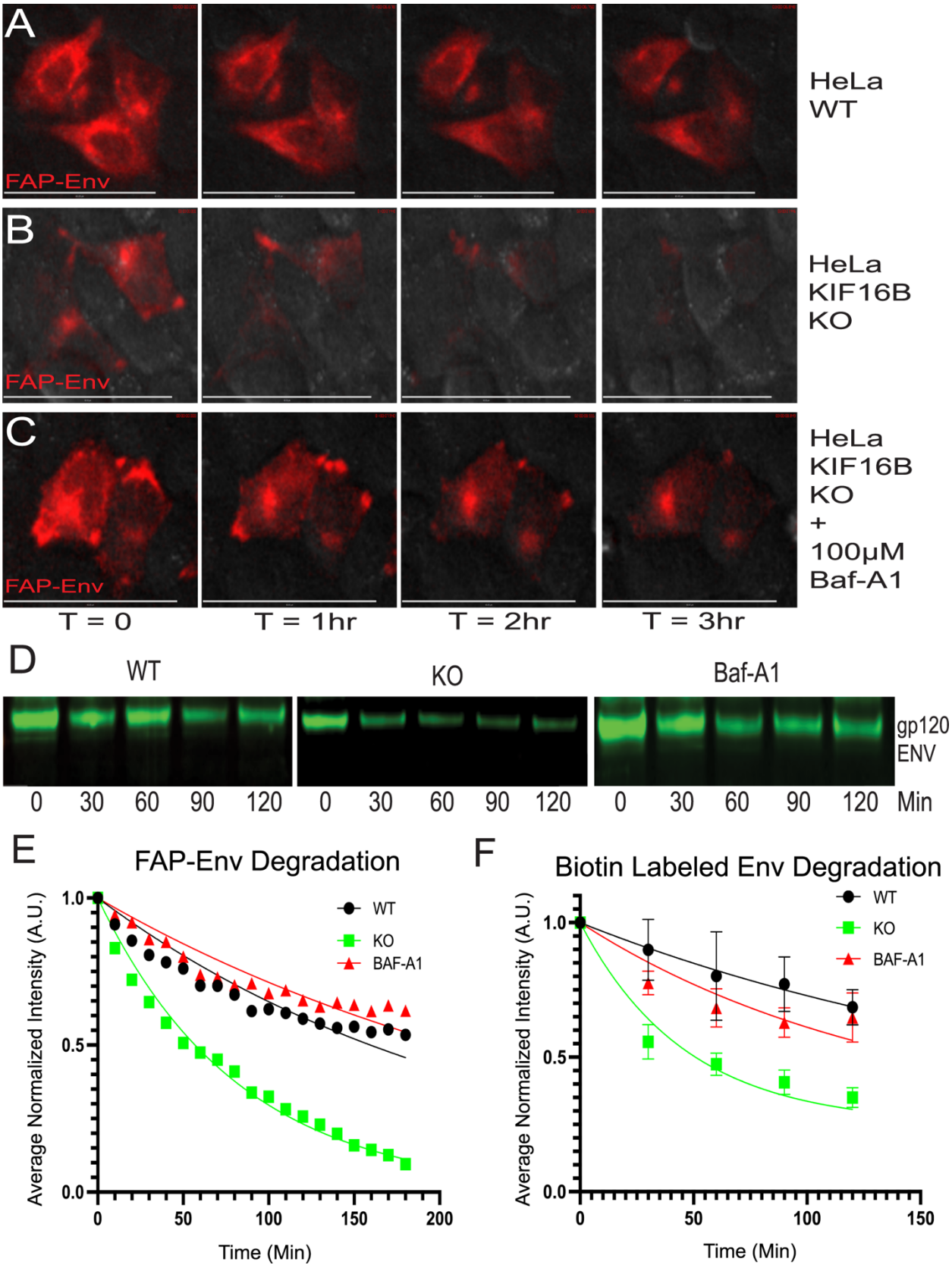
A
FAP-Env
HeLa
WT
B
FAP-Env
HeLa
KIF16B
KO
C
FAP-Env
HeLa
KIF16B
KO
+
100μM
Baf-A1
T = 0
T = 1hr
T = 2hr
T = 3hr
D
WT
KO
Baf-A1
gp120
ENV
0 30 60 90 120 0 30 60 90 120 0 30 60 90 120 Min
E
FAP-Env Degradation
Average Normalized Intensity (A.U.)
1.0
0.5
0.0
0 50 100 150 200
Time (Min)
WT
KO
BAF-A1
F
Biotin Labeled Env Degradation
Average Normalized Intensity (A.U.)
1.0
0.5
0.0
0 50 100 150
Time (Min)
WT
KO
BAF-A1

781

782 **FIG 4** KIF16B KO leads to enhanced degradation of endocytosed Env in the lysosome.
783 (A, B, C) Frames from live cell movies for Fap-Env expressed in (A) WT HeLa cells with
784 vehicle DMSO; (B) KIF16B KO cells with DMSO; or (C) KIF16B KO cells with 100μM Baf-
785 A1. Representative frames are shown for each hour over the time course. (B) Western
786 blots shown are biotinylated Env from surface-labeled cells, with lysates chased over the
787 time course, pulled down with streptavidin beads, and blotted for Env. Labels indicate
788 WT, KIF16B KO, and KIF16B KO + Baf-A1 HeLa cells. (C) Quantification of signal
789 intensity of each time point over the FAP-Env imaging experiment normalized to first
790 frame. (D) Quantification of the Western blot signal for each time point for biotin-
791 streptavidin pulse-chase experiment. Error bars represent SD from 5 independent
792 experiments. Fit curves for both C and D were generated using the Prism 9 non-linear
793 regression one-phase decay algorithm. Bars represent 60 μm.

794

795

796

797

798

799

800

801

802

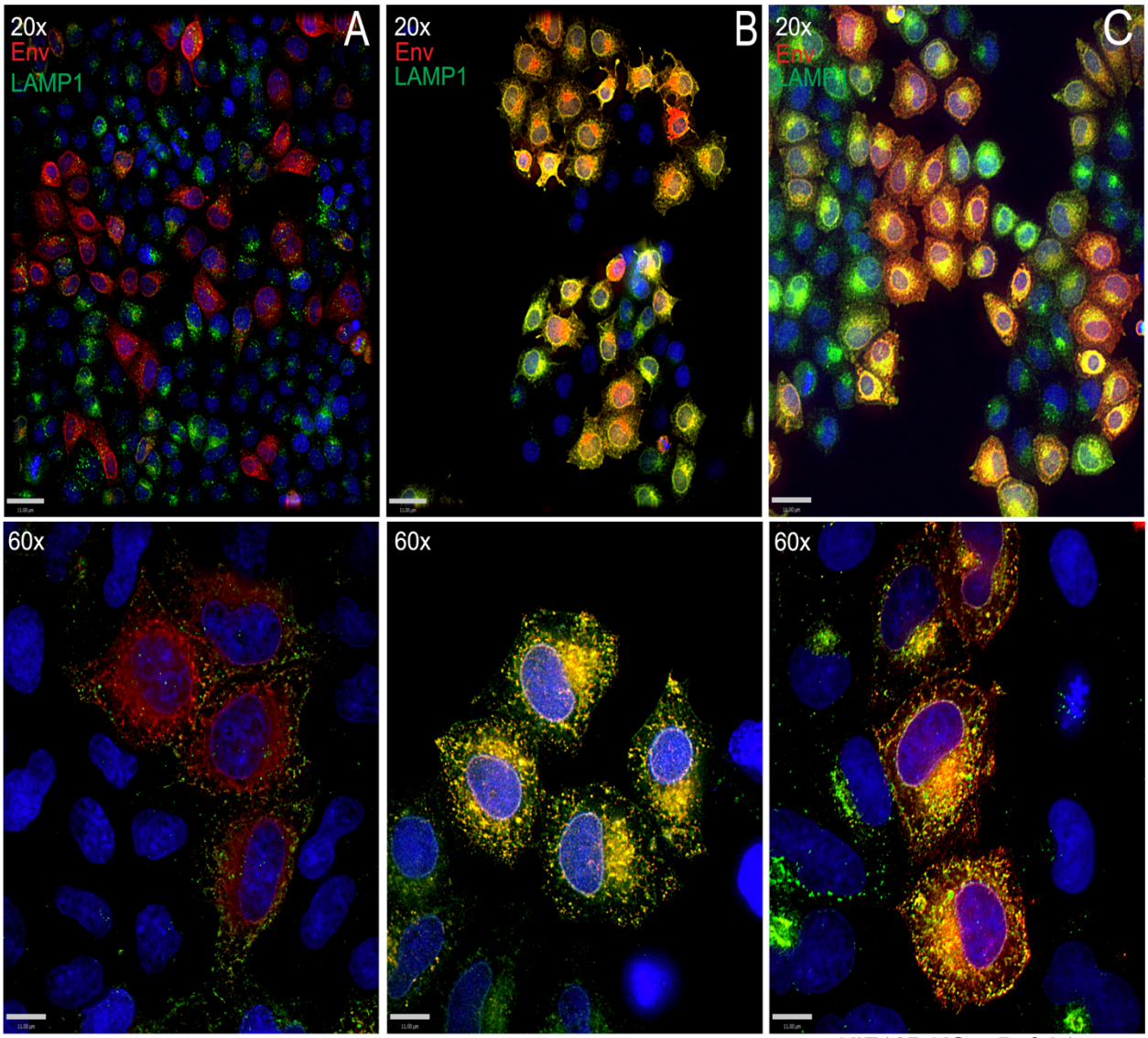

WT HeLa KIF16B KO KIF16B KO + Baf-A1

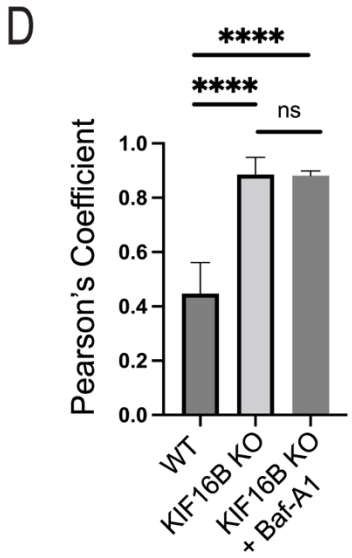

803

804 **FIG 5** KIF16B KO shunts Env to lysosomal compartments. (A) HIV-1 NL4-3 Env
805 expressed in WT HeLa cells. Top image 20x magnification, bottom image 60x. (B) NL4.3
806 expressed in KIF16B KO HeLa cells. Top image 20x magnification, bottom image 60x.
807 (C) NL4-3 expressed in KIF16B KO HeLa cells with Baf-A1 added for 3 hours prior to
808 imaging. For all imaging, cells were fixed and immunolabeled for Env with 2G12 antibody
809 and for endogenous LAMP1 with H4A3 antibody. (D) Pearson's correlation coefficient
810 showing the degree of colocalization between Env and LAMP1 positive compartments
811 between WT, KIF16B KO cells, and WT cells with Baf-A1 in A, B, and C, respectively.
812 Pearson's correlation coefficient equation using Volocity 6.5.1 software after manual
813 thresholding. Unpaired t-test performed on Prism 9 to get significance values for
814 difference in colocalization. ****, $P < 0.0001$; *, $P = 0.0155$. Bars represent 11μm.

815

816

817

818

819

820

821

822

823

824

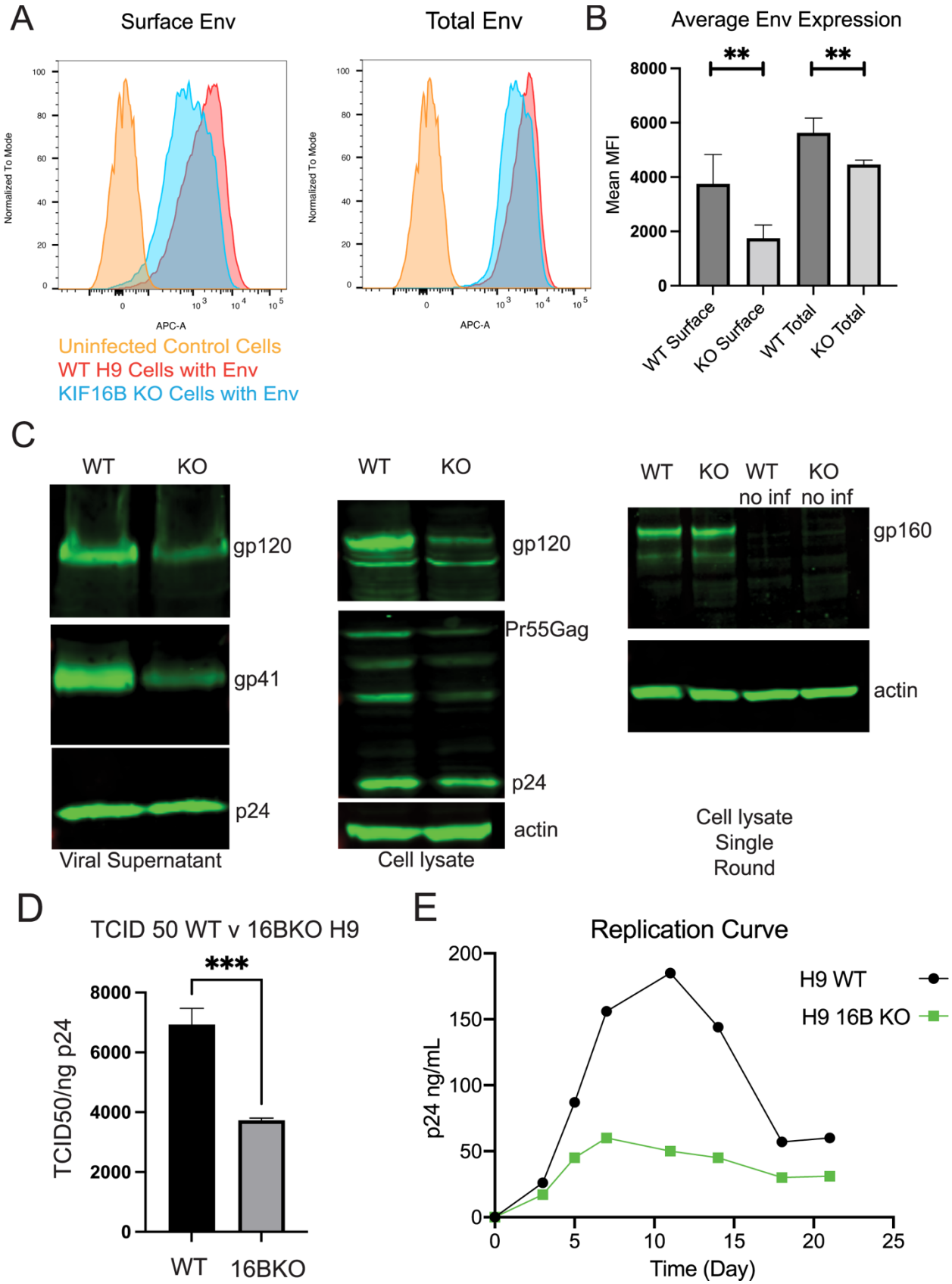
A
Surface Env
Total Env
Normalized To Mode
APC-A
Uninfected Control Cells
WT H9 Cells with Env
KIF16B KO Cells with Env
B
Average Env Expression
Mean MFI
**
**
WT Surface
KO Surface
WT Total
KO Total
C
WT
KO
gp120
gp41
p24
Viral Supernatant
WT
KO
gp120
Pr55Gag
p24
actin
Cell lysate
WT
KO
WT no inf
KO no inf
gp160
actin
Cell lysate Single Round
D
TCID 50 WT v 16BKO H9
***
TCID50/ng p24
WT
16BKO
E
Replication Curve
p24 ng/mL
Time (Day)
H9 WT
H9 16B KO

825

826 **FIG 6** KIF16B depletion leads to reduction of Env on the cell surface, particle
827 incorporation, infectivity, and viral replication. (A) Flow plots for cell surface staining (non-
828 permeabilized) and total Env content (permeabilized) in WT H9 and KIF16B KO H9 cells.
829 Cells were fixed and stained for Env using anti-gp120 2G12 antibody. (B) Quantification
830 of flow cytometry mean fluorescent intensity of Env expression on surface and total cell
831 averaged across 5 independent experiments. Unpaired t-test performed on Prism 9 to get
832 significance values between surface vs total. **, $P < 0.005$ (C) WT and KIF16B H9 cells
833 were infected with VSV-G-pseudotyped NL4-3. Shown are Western blots of Env and Gag
834 content for particles in viral supernatant (left) and cell lysates (middle) collected on day 5
835 following infection. Note that loading was normalized for p24 content (supernatants) or
836 for total cellular protein (cell lysates). Rightmost blot, single-round infection of WT and
837 KIF16B KO H9 cells infected with VSV-G-pseudotyped NL4-3 at an MOI of 0.5 and
838 harvested for cell lysate analysis after 24 hours. Uninfected WT and KO cell lysates were
839 run on the same blot as controls. Blotting was performed with 2G12 antibody against HIV-
840 1 gp160 and ACTN05 (Invitrogen) against actin as a loading control. (D) Infectivity of viral
841 particles released from WT or KIF16B KO H9 cells from 3 independent experiments
842 evaluated using TZM-bl indicator cells. (E) WT (black line) and KIF16B KO (green line)
843 were infected with VSV-G-pseudotyped NL4-3 virus. Viral growth was monitored over
844 time by detection of p24 in the culture supernatant.

845

846

847

848

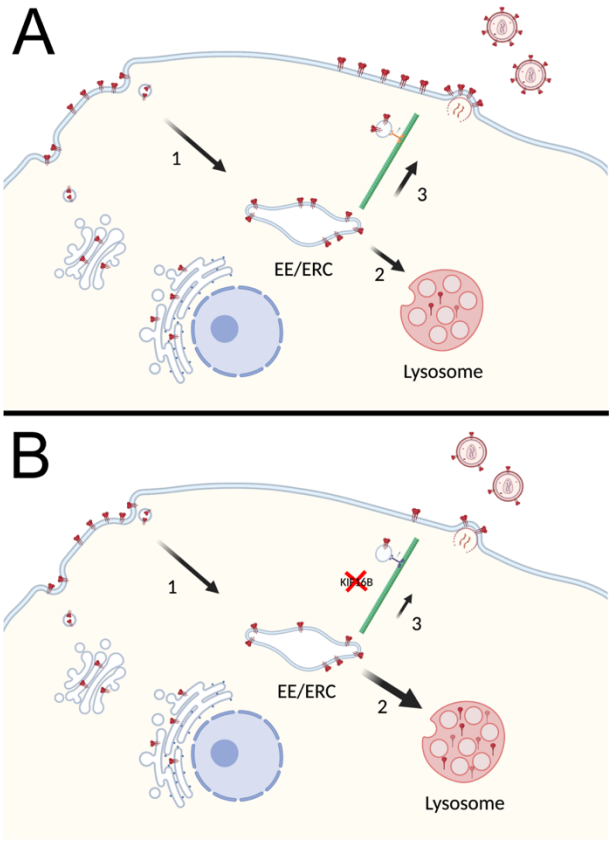

849

850 **FIG 7** Model of Env Trafficking with (A) and without (B) KIF16B. (A) In a wild-type cell,
851 Env is produced in the rough endoplasmic reticulum and follows the secretory pathway
852 to the cell surface. Env is then endocytosed into early endosomes (path #1 in the figure),
853 which later may sort to the endosomal recycling compartment (ERC) for recycling. This
854 compartment is depicted as “EE/ERC”. A fraction of Env in EEs can progress to fuse with
855 lysosomes, leading to lysosomal degradation in path #2. In path #3, Env is directed in an
856 anterograde manner to the PM, where it is available for incorporation into viral particles.
857 Path #3 is the relevant pathway that is partially dependent upon KIF16B. (B) In a cell with
858 KIF16B KO, a diminished fraction of Env is delivered to the PM from the EE/ERC via path
859 #3. This results in an increase in the amount of Env shunted to the lysosome (path #2,

860 illustrated as broader arrow) and enhanced degradation of Env. The change in the
861 distribution of endocytosed Env is shown graphically as fewer trimers on the budding and
862 mature virion, as well as fewer trimers on the PM and more trimers in the lysosome. Figure
863 created with BioRender.com.

864

865

866

867

868

869

870

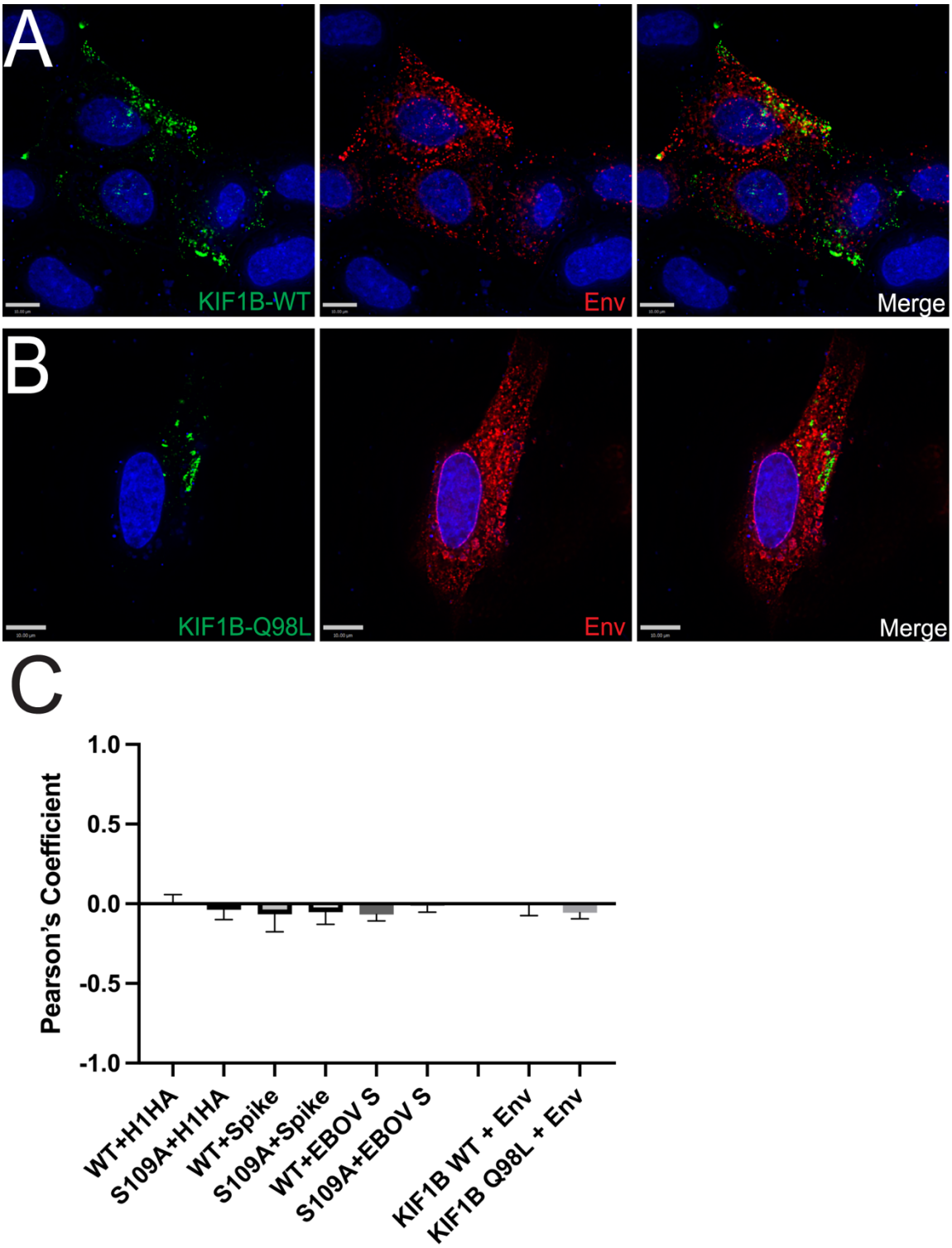
A
KIF1B-WT
Env
Merge
B
KIF1B-Q98L
Env
Merge
C
Pearson's Coefficient
1.0
0.5
0.0
-0.5
-1.0
WT+H1HA
S109A+H1HA
WT+Spike
S109A+Spike
WT+EBOV S
S109A+EBOV S
KIF1B WT + Env
KIF1B Q98L + Env

871

872

873

874 **Fig S1** (A, B) Coexpression of KIF1B WT and KIF1B Q98L (dominant-negative) with HIV-
875 1 Env. Cells were fixed and immunostained with 2G12 antibody specific to the Env
876 glycoprotein. Green, KIF1B; red, Env; rightmost image, overlay. (C) Degree of
877 colocalization for all viral glycoproteins included in Fig 2 with KIF16B (left six bars); and
878 colocalization of Env with KIF1B (rightmost two bars), measured by Pearson's correlation
879 coefficient equation using Volocity 6.5.1 software after thresholding. Results are shown
880 as means ± SD from a total of 5 representative images. Bars represent 10 μm.

881

882

883

884

885

886

887

888

889

890

891

892

893

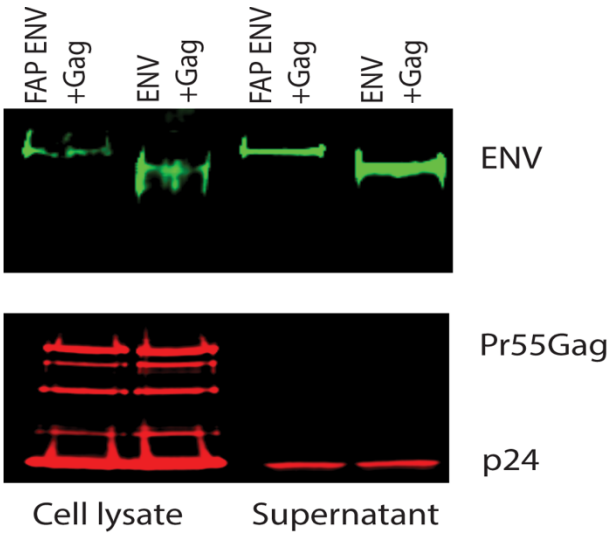

894

895 **Fig S2** FAP-tagged Env or WT JR-FL Env were co-expressed with Env-deficient provirus.
896 Western blot shows Env in cell lysates and on pelleted particles from supernatants. Env
897 was blotted with 2G12 and Gag detected with CA183.

898

899

900

901

902

903

904

905

906

907

A

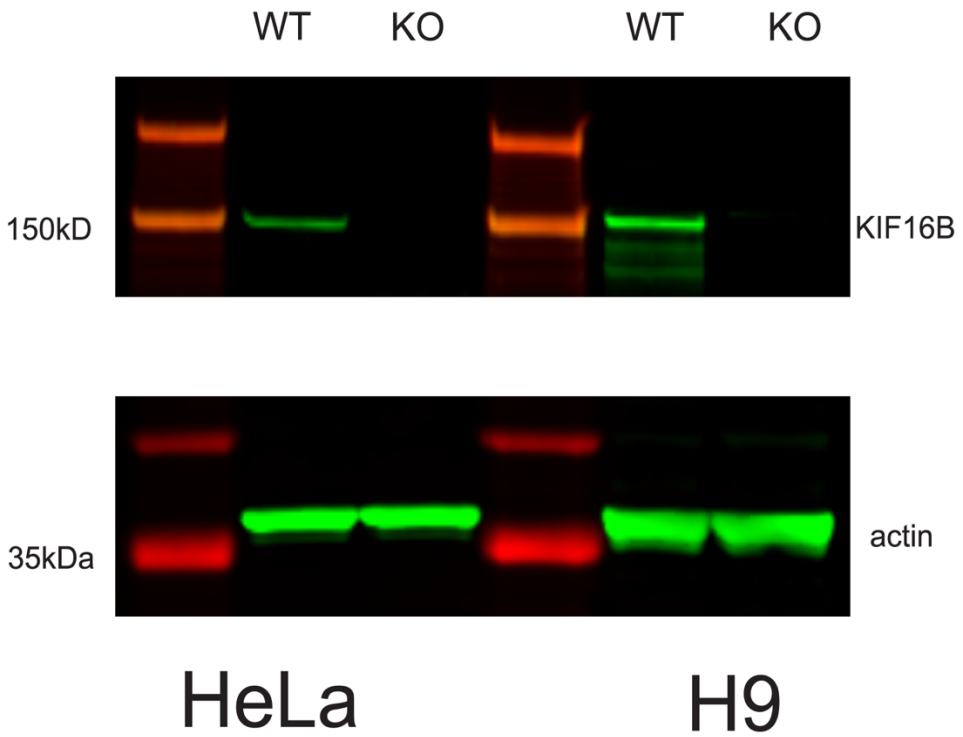
WT
KO
WT
KO
150kD
KIF16B
35kDa
actin
HeLa
H9

B

Status
Succeeded
Guide Target
CTCACGGATAAGTTTGACGT
PAM Sequence
TGG
Indel %
91
Model Fit (R^2)
0.91
Knockout-Score
76
EDITED SAMPLE 150 TO 215 BP
CONTROL SAMPLE 149 TO 214 BP

912 **Fig S3** (A) Representative blots of WT and KIF16B KO HeLa (left) and H9 (right) cell lines
913 blotted for KIF16B and actin loading control showing complete protein knock out in both
914 cell lines. (B) Sequence of genomic DNA from HeLa cells showing CRISPR-Cas9 indel.
915 Dotted line indicates cut site of CRISPR-Cas9 complex. Edited sample sequence on top
916 for KIF16B KO cells, the control sample on bottom was the reference sequence from WT
917 cells that were the same cells used to make the knockout clones. Sequence analyzed by
918 ICE analysis via the Synthego software application.

919